TF-SSD: A Strong Pipeline via Synergic Mask Filter for Training-free Co-salient Object Detection

Zhijin He[1*] Shuo Jin[1,2*] Siyue Yu[1†] Shuwei Wu[1] Bingfeng Zhang[3] Li Yu[4] Jimin Xiao[1]
[1]XJTLU [2]University of Liverpool [3]China University of Petroleum (East China)
[4]Nanjing University of Information Science and Technology
{Zhijin.He24, Shuwei.Wu24}@student.xjtlu.edu.cn, shuo.jin@liverpool.ac.uk,
{siyue.yu02, jimin.xiao}@xjtlu.edu.cn, bingfeng.zhang@upc.edu.cn, li.yu@nuist.edu.cn

Abstract

*Co-salient Object Detection (CoSOD) aims to segment salient objects that consistently appear across a group of related images. Despite the notable progress achieved by recent training-based approaches, they still remain constrained by the closed-set datasets and exhibit limited generalization. However, few studies explore the potential of Vision Foundation Models (VFMs) to address CoSOD, which demonstrate a strong generalized ability and robust saliency understanding. In this paper, we investigate and leverage VFMs for CoSOD, and further propose a novel training-free method, TF-SSD, through the synergy between SAM and DINO. Specifically, we first utilize SAM to generate comprehensive raw proposals, which serve as a candidate mask pool. Then, we introduce a quality mask generator to filter out redundant masks, thereby acquiring a refined mask set. Since this generator is built upon SAM, it inherently lacks semantic understanding of saliency. To this end, we adopt an intra-image saliency filter that employs DINO's attention maps to identify visually salient masks within individual images. Moreover, to extend saliency understanding across group images, we propose an inter-image prototype selector, which computes similarity scores among cross-image prototypes to select masks with the highest score. These selected masks serve as final predictions for CoSOD. Extensive experiments show that our TF-SSD outperforms existing methods (*e.g.*, 13.7% gains over the recent training-free method). Codes are available at https://github.com/hzz-yy/TF-SSD.*

1. Introduction

Co-salient Object Detection (CoSOD) is an emerging computer vision task that extends traditional Salient Object Detection (SOD) to identify common salient objects across multiple related images [7, 43]. The key challenge is to ensure the models can identify visual consensus across images, instead of relying on class-specific semantic patterns.

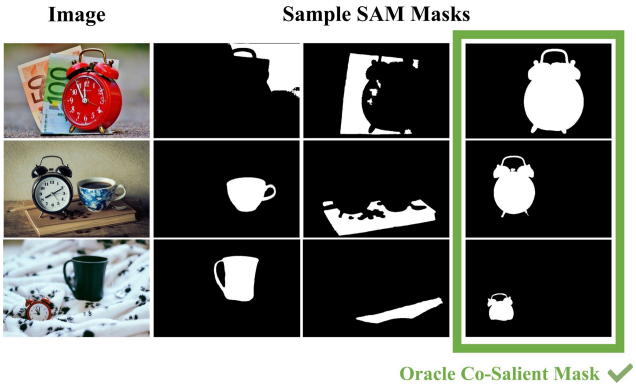

Figure 1. Segmentation results derived from SAM. The oracle masks selected under the ground truth guidance exhibit co-salient representations, which are highlighted in the green rectangle.

Existing state-of-the-art (SOTA) methods follow the training-based paradigm and have achieved impressive performance. However, they are mostly trained on closed-set datasets and exhibit limited generalization [34]. These problems exhibit a fundamental mismatch: CoSOD requires discovering generalizable visual consensus across objects, while conventional supervised methods often overfit to biased class distributions of the training set.

Recent advances in vision foundation models (VFM), such as SAM [15], and DINO [2, 25], have opened new avenues for various vision tasks. SAM exhibits an impressive generalization ability for image segmentation. As depicted in Fig. 1, SAM generates numerous masks, which contain co-salient objects with accurate delineation. It motivates us to explore the potential of SAM for CoSOD. Further, we conduct an experiment to quantify SAM's segmentation

*Equal contribution.
†Corresponding author: siyue.yu02@xjtlu.edu.cn

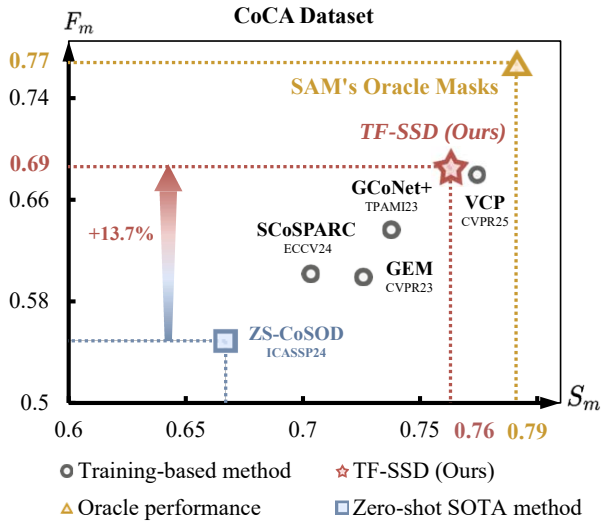

Figure 2. Comparison of our TF-SSD and other CoSOD methods. F_m and S_m denote the F-measure and S-measure, respectively. Our method surpasses training-based methods and achieves 13.7% improvement over the recent training-free SOTA method.

ability in CoSOD benchmarks. As shown in Fig. 2, when selecting oracle masks[1] from SAM's outputs, the segmentation performance on CoCA benchmark [44] outperforms all existing SOTA methods, including fully-supervised approaches [9, 19, 33, 42, 48]. This upper bound result suggests that SAM's segmentation capability is sufficient for CoSOD. However, SAM inherently lacks the semantic understanding required to distinguish cross-image relationships and to determine the co-salient predictions. This gap reveals a crucial question: '*How to capture common semantics for identifying accurate co-salient masks from SAM's exhaustive proposals?*'

To address this, we turn to the self-supervised VFM, DINO [2], which has demonstrated an exceptional ability to extract rich and salient semantic features. Its dense features and attention maps exhibit strong semantic coherence for salient objects [25, 29], which provides accurate semantic understanding that naturally complements SAM's segmentation results. Such a phenomenon enables a mutually complementary paradigm: DINO's semantic guidance can address SAM's stochastic nature in mask generation, while SAM's precise boundary perception enhances DINO's coarse localization. Building on these insights, we introduce a novel **T**raining-**F**ree approach for CoSOD through the **S**ynergy between **SAM** and **DINO**, termed **TF-SSD**. Our core strategy is to treat SAM's exhaustive mask proposals as a rich candidate mask pool and progressively refine them through complementary guidance of DINO at two levels: intra-image visual saliency and inter-image semantic consistency.

Specifically, our TF-SSD utilizes a progressive pipeline including three components. Since SAM typically generates numerous mask proposals for salient foreground objects, including multiple extremely small and overlapping masks, we first propose a **Quality Mask Generator (QMG)** to progressively filter out these low-quality and redundant masks based on intrinsic properties, such as area and size, to obtain the refined mask proposal set. Nevertheless, QMG can't distinguish the visually salient object within each image. We thus introduce an **Intra-image Saliency Filter (ISF)**. It leverages DINO's attention maps to identify visually salient masks by evaluating the spatial alignment between attention responses and mask regions. However, these operations are limited to individual images, failing to capture the co-existing relationships inside the group. We further propose an **Inter-image Prototype Selector (IPS)** for inter-image semantic consistency. In detail, IPS computes similarity scores among inter-image prototypes, which are established by the masks from our ISF and global features from DINO. The masks with the highest score in each image are then selected as the final co-salient predictions for CoSOD.

These components work in concert and effectively boost the performance of CoSOD. As shown in Fig. 2, our TF-SSD outperforms existing training-based methods and surpasses the recent training-free method up to 13.7% in F-measure on the CoCA benchmark. In summary, our contributions are concluded as follows:

- We propose a novel training-free framework, TF-SSD, for CoSOD. It progressively transforms SAM's exhaustive mask proposals into co-salient mask predictions under the guidance of DINO's feature representation.
- We propose QMG and ISF to filter high-quality mask proposals and detect visually salient masks within each image based on intra-image visual saliency. To facilitate co-salient understanding across images, IPS is introduced to model inter-image prototype relations and select semantically consistent masks as the final CoSOD predictions.
- Extensive experiments on CoSOD benchmarks show that TF-SSD achieves SOTA performance, which outperforms both training-based and training-free approaches.

2. Related Works

2.1. Co-salient Object Detection

CoSOD requires segmenting salient objects that are commonly present across a group of images. Recent advances have achieved significant progress, and existing methods can be categorized into supervised [9, 11, 16, 17, 19, 30, 33, 35, 42, 45, 46, 48], unsupervised [1, 4, 12, 21, 23, 32, 37], and zero-shot [34] paradigms.

Most supervised methods follow a three-stage paradigm

[1]We select the best mask result from SAM's top-10 predictions using ground truth (GT) mask guidance, which are shown in Fig. 1.

including feature encoding , consensus extraction and dispersion, and final prediction. Some methods actively model both the commonality and the distinction between groups. GCoNet+ [45] introduces a group collaborative learning framework, which leverages negative relations between groups to learn more discriminative features. VCP [31] proposes embedding the extracted visual consensus into prompts, which forms a prompt tuning approach with minimized tunable parameters.

To address annotation dependency, unsupervised solutions [1, 4, 32] are explored to learn co-salient objects solely from unlabeled data. SCoSPARC [3] introduces a two-stage self-supervised model involving a novel confidence-based adaptive threshold, which enhances cross-image feature correspondence. Moreover, the zero-shot paradigm has advanced with the emergence of vision foundation models. ZS-CoSOD [34] pioneers this research direction by integrating powerful foundation models to generate custom group prompts that represent the co-salient objects to guide SAM in predicting results for CoSOD in a training-free manner. PAP-SAM [39] further introduces a global-local prior adaptive perception strategy to enhance SAM for CoSOD. However, few studies have explored how to endow the coarse segmentation results derived from SAM with co-salient semantic understanding.

2.2. Vision Foundation Model

Building upon large-scale high-quality datasets [5, 15, 25, 28, 36], learning generalized visual representations has become a popular paradigm in computer vision. Vision Foundation Models (VFMs) aim to undergo pre-training on large-scale datasets to learn general visual representations, which can generalize to diverse downstream tasks, including image-level recognition [18, 26], pixel-level perception [6, 14, 24], and video restoration [13, 22].

One research branch of VFM is self-supervised models [10, 47], which aim to learn general visual features solely from images. Among these, the DINO series [2, 25, 29] have shown impressive capabilities to capture explicit details in their dense features, while its attention map can localize the precise foreground object. Another research branch of VFM is the SAM series [15, 27], which are generally pre-trained on a large-scale annotated training set in a fully-supervised paradigm. SAM [15] has demonstrated impressive zero-shot, class-agnostic segmentation ability for general image segmentation tasks. To address CoSOD in a training-free manner, we turn to VFMs that generate comprehensive mask proposals and filter the co-salient ones through the synergy between SAM and DINO.

3. Methodology

The overview pipeline of our TF-SSD is presented in Sec. 3.1, which comprises three key components: 1) Quality Mask Generator (QMG) in Sec. 3.2; 2) Intra-image Saliency Filter (ISF) in Sec. 3.3; and 3) Inter-image Prototype Selector (IPS) in Sec. 3.4.

3.1. Overview

Given a group of N images $\mathcal{I} = \{I_1, I_2, \ldots, I_n\}$ that contain salient objects of a common category across the group. CoSOD seeks to identify co-salient objects and generate corresponding segmentation masks $\mathcal{Y} = \{Y_n\}_{n=1}^{N}$. Our framework operates through a progressive pipeline that narrows SAM's masks to co-salient predictions for CoSOD, as shown in Fig. 3. The overall pipeline is as follows:

1) For each image $I_n \in \mathcal{I}$, SAM is first used to generate comprehensive segmentation proposals $\mathbf{M}_n^{raw}$. Then, our QMG employs a multi-stage strategy to filter out redundant masks, obtaining refined masks $\mathbf{M}_n^{refine}$.
2) Next, owing to the absence of visual saliency perception in $\mathbf{M}_n^{refine}$ within a single image, our ISF employs attention maps from DINO to highlight visually salient regions. It filters masks with low saliency scores using an adaptive threshold, yielding the filtered masks $\mathbf{M}_n^{salient}$.
3) Subsequently, since most images contain multiple salient objects, our IPS extracts prototypes from each mask $m_{n,t} \in \mathbf{M}_n^{salient}$ to compute the co-salient scores. Finally, masks with the highest co-salient score are selected as the final prediction $\mathcal{Y}$ for CoSOD.

3.2. Quality Mask Generator

Quality Mask Generator (QMG) serves as the foundation of our framework, which transforms SAM's exhaustive mask proposals into a refined mask proposal set, prepared for co-salient detection. Given an input image I_n, SAM initially generates a raw mask set $\mathbf{M}_n^{raw} = \{m_{n,1}^{raw}, m_{n,2}^{raw}, \ldots, m_{n,T_o}^{raw}\}$ where T_o denotes the mask number of each image. However, the nature of the SAM generation process introduces significant limitations: most masks correspond to unrelated objects and redundant segments of the same object.

To address this, QMG progressively eliminates trivial, overlapping, and excessively sized masks. This process operates through: SAM-based initial filtering, overlap filtering, and quality assessment, summarized in Algorithm 1 for a clear view.

SAM-based Initial Filtering. First, $\mathbf{M}_n^{raw}$ contains many masks with excessively small area of the segment, termed trivial masks. We posit that these masks are not associated with salient objects. To discard these trivial masks, we compute an area ratio $r_{n,t}^{area}$, which denotes the proportion of the image covered by the mask, formulated as:

$$r_{n,t}^{area} = \frac{|m_{n,t}^{raw}|}{H \times W}, \tag{1}$$

where $|m_{n,t}|$ denotes the foreground spatial area of the

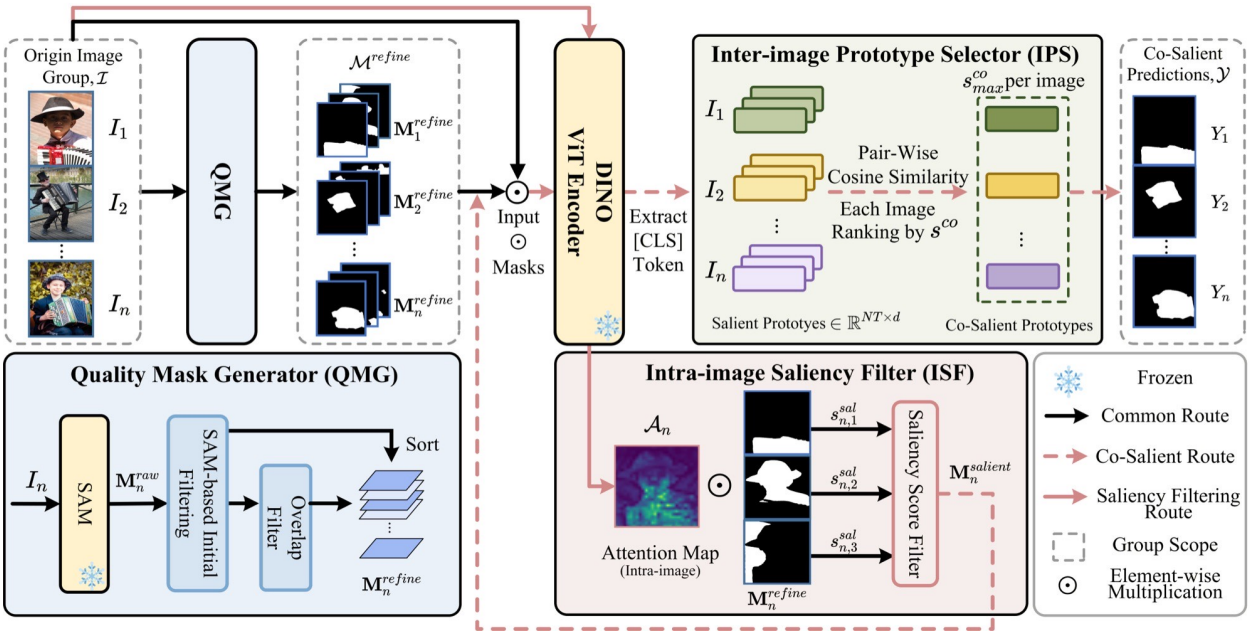

Figure 3. Overview pipeline of our TF-SSD. It contains four components: a Quality Mask Generator (QMG) that filters out exhaustive candidate masks from SAM, a DINO encoder for salient attention and semantic prototype extraction, an Intra-image Saliency Filter (ISF) for visually salient purification within a single image, and an Inter-image Prototype Selector (IPS) that builds the saliency relationship across group images to discover the co-salient masks as the final predictions for CoSOD. For clarity, our notations are defined as: $m_{n,t}$ denotes an individual mask, $\mathbf{M}_n$ denotes the mask set of image n (e.g., $\mathbf{M}_n^{raw}$, $\mathbf{M}_n^{refine}$).

mask $m_{n,t}^{raw}$, H and W denotes the image height and width. $r_{n,t}^{area}$ is used to filter out trivial masks, establishing the coarse mask set $\mathbf{M}_n^{coarse}$, as formulated:

$$\mathbf{M}_n^{coarse} = \{\, m_{n,t}^{raw} \mid r_{n,t}^{area} \geq \tau_{area} \,\}, \tag{2}$$

where τ_{area} is the area threshold.

Overlap Filtering. Besides the above trivial masks, there also exist multiple overlapping segments. Therefore, an overlap filtering is introduced to further purify $\mathbf{M}_n^{coarse}$.

We design the overlap ratio $\rho_{i\to j}$ for each mask pair:

$$\rho_{i\to j} = \frac{|m_{n,i} \cap m_{n,j}|}{|m_{n,j}|}, \tag{3}$$

where $m_{n,i}$ and $m_{n,j}$ denote paired masks. To preserve larger masks, we calculate the overlap ratio of the candidate mask from $\mathbf{M}_n^{coarse}$ in ascending order of mask area. If the current mask has a high overlap ratio ($\rho_{i\to j} \geq \tau_{con}$, τ_{con} is the overlap threshold) with any larger mask, it is removed. The rest masks are formed as the purified set $\mathbf{M}_n^{purified}$.

Quality Assessment. While the preceding area-based filtering is can filter most extreme small and overlapping masks, there are still plenty of noisy masks in $\mathbf{M}_n^{purified}$. Thus, we further leverage the IoU score $\text{IoU}_{n,t}^{pred}$ to filter the trivial masks as an auxiliary. Note that SAM predicts the IoU score to measure the prediction quality. We compute a quality-based metric by combining the IoU score and our area ratio.

First, given that salient objects typically have moderate sizes rather than extreme ones, we define an area score $S_{n,t}^{area}$ to assign lower scores to masks with excessive sizes:

$$S_{n,t}^{area} = \begin{cases} 1.0 & \text{if } r_{min} \leq r_{n,t}^{area} \leq r_{max}, \\ r_{n,t}^{area}/r_{min} & \text{if } r_{n,t}^{area} < r_{min}, \\ \mathcal{P}(r_{n,t}^{area}) & \text{if } r_{n,t}^{area} > r_{max}, \end{cases} \tag{4}$$

where $\mathcal{P}(r_{n,t}^{area}) = \max(\sigma, 1.0 - (r_{n,t}^{area} - r_{max}) \times \gamma)$ is a penalty function with hyper-parameters σ and γ. It progressively assigns lower scores as the area increases to suppress masks that exceed the ideal size. Eq. 4 assigns the highest score to masks belonging to the ideal size $[r_{min}, r_{max}]$.

Then, we integrate $S_{n,t}^{area}$ with $\text{IoU}_{n,t}^{pred}$, to compute a balanced quality score $S_{n,t}^{ba}$, as

$$S_{n,t}^{ba} = \alpha \cdot \text{IoU}_{n,t}^{pred} + \beta \cdot S_{n,t}^{area}, \tag{5}$$

where α and β are weighted factors to balance prediction confidence and size preferences. A higher $S_{n,t}^{ba}$ means the quality of the mask is better.

Finally, according to the quality score, the top T_r masks from $\mathbf{M}_n^{purified}$ are selected to constitute the QMG's final output $\mathbf{M}_n^{refined} = \{m_{n,t}^{refined}\}_{t=1}^{T_r}$.

Algorithm 1 Quality Mask Generator (QMG)

Input: A group of images $\mathcal{I} = \{I_n\}_{n=1}^{N}$
Output: Refined mask sets $\mathcal{M}^{refine} = \{\mathbf{M}_n^{refine}\}_{n=1}^{N}$
Initialize: $\mathbf{M}_n^{coarse}$, $\mathbf{M}_n^{purified}$, $\mathbf{M}_n^{scored}$, $\mathbf{M}_n^{refine}$, $\mathbf{M}_n^{raw}$
for $I_n \in \mathcal{I}$:
  $\mathbf{M}_n^{raw} \leftarrow \text{SAM}(I_n)$
  Stage.1
    for $m_{n,t}$ **in** $\mathbf{M}_n^{raw}$:
      Compute area ratio $r_{n,t}^{area}$ (Eq. 1)
      if $r_{n,t}^{area} \geq \tau_{area}$:
        Add $m_{n,t}$ to $\mathbf{M}_i^{coarse}$
  end
  Stage.2
    Sort $\mathbf{M}_n^{coarse}$ by mask area (descending)
      for $m_{n,i}$, $m_{n,j}$ **in** $\mathbf{M}_n^{coarse}$:
        Calculate $\rho_{i \to j}$ (Eq. 3)
        if $\rho_{i \to j} < \tau_{con}$:
          Add $m_{n,i}$ to $\mathbf{M}_n^{purified}$
  end
  Stage.3
    for $m_{n,t}$ **in** $\mathbf{M}_n^{purified}$:
      Compute area score $S_{n,t}^{area}$ (Eq. 4)
      Compute balanced score $S_{n,t}^{ba}$ (Eq. 5)
    Sort $\mathbf{M}_n^{purified}$ by $S_{n,t}^{ba}$
    Select top T_r masks to form $\mathbf{M}_n^{refined}$
  end
  Add $\mathbf{M}_n^{refined}$ to $\mathbf{M}^{refined}$
return $\mathcal{M}^{refined}$

3.3. Intra-image Saliency Filter

While QMG produces refined segmentations $\mathbf{M}_n^{refine}$, it lacks salient semantic awareness within images. In contrast, recent works have demonstrated that attention maps from DINO naturally highlight salient objects without explicit supervision. Hence, we propose an Intra-image Saliency Filter (ISF), which leverages DINO's attention representation to select masks corresponding to salient regions.

Specifically, given an image I_n, we can extract the attention map $\mathcal{A}_n \in [0, 1]$ of the [CLS] token from DINO's ViT encoder, which is reshaped to $\mathcal{A}_n \in \mathbb{R}^{h \times w}$, where h and w are the height and width. $\mathcal{A}_n$ can highlight visually salient regions with higher response intensity, as shown in the second diagram of the first row of Fig. 4.

As a result, for each mask proposal $m_{n,t}^{refine} \in \mathbf{M}_n^{refine}$, we compute its saliency score $s_{n,t}^{sal}$ based on the attention response within the masked region, formulated as:

$$s_{n,t}^{sal} = \frac{1}{|m_{n,t}^{refine}|} \sum \mathcal{A}_n(x, y) \odot m_{n,t}^{refine}(x, y), \quad (6)$$

where $|m_{n,t}^{refine}|$ denotes the spatial area of $m_{n,t}^{refine}$, (x, y) represents spatial location, and $\odot$ denotes the element-wise multiplication. $s_{n,t}^{sal}$ reflects how well the mask region aligns with the salient representation, which is shown in the third row of Fig. 4. A higher $s_{n,t}^{sal}$ means that the alignment is better and thus the corresponding mask tends to be a salient mask. We select the Top T masks $\mathbf{M}_n^{refine}$ based on the saliency score to form the salient mask set $\mathbf{M}_n^{salient} = \{m_{n,t}^{salient}\}_{t=1}^{T}$.

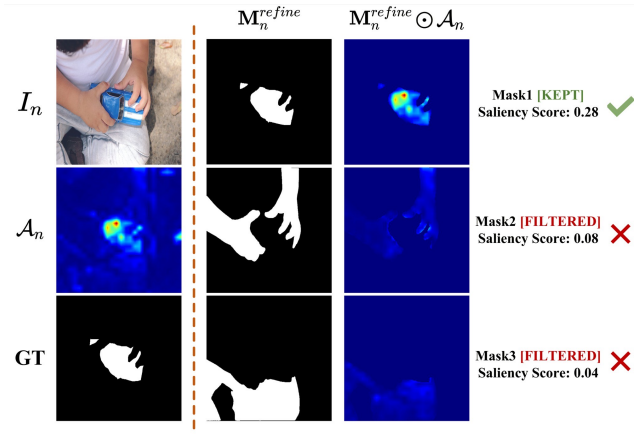

Figure 4. Illustration of Intra-image Saliency Filter. **Row 1**: Original image, self-attention map of DINO, and ground truth. **Row 2**: Three mask proposals generated by QMG. **Row 3**: Attention response obtained by element-wise multiplication of each mask with the attention map. Mask 1 achieves a high saliency score due to strong overlap between salient regions and the mask proposal, while Masks 2 and 3 receive low scores due to non-overlap.

3.4. Inter-image Prototype Selector

While ISF successfully identifies salient regions within individual images, it cannot determine which of these salient objects are co-salient across the entire image group. Therefore, we propose an Inter-image Prototype Selector (IPS) that establishes semantic prototypes for each mask in $\mathbf{M}_n^{salient}$ using DINO and matches their consistency across the image group to identify the co-salient masks.

The total process is demonstrated in Fig. 5, for each mask $m_{n,t} \in M_n^{salient}$, we first extract its prototype $p_{n,t}$ using a feature extraction function $\mathcal{F}$:

$$p_{n,t} = \mathcal{F}(I_n \odot m_{n,t}), \quad (7)$$

where $\mathcal{F}(\cdot)$ means extracting the [CLS] token from DINO's ViT encoder, and $p_{n,t} \in \mathbb{R}^{1 \times d}$ (d is the channel size). This process generates a set of prototypes $P \in \mathbb{R}^{NT \times d}$, where NT means N image in the given group and each has T salient masks derived from our ISF.

Then, the pair-wise cosine similarity matrix $C \in \mathbb{R}^{NT \times NT}$ is computed by:

$$C = \frac{PP^{\top}}{\|P\|^2}. \quad (8)$$

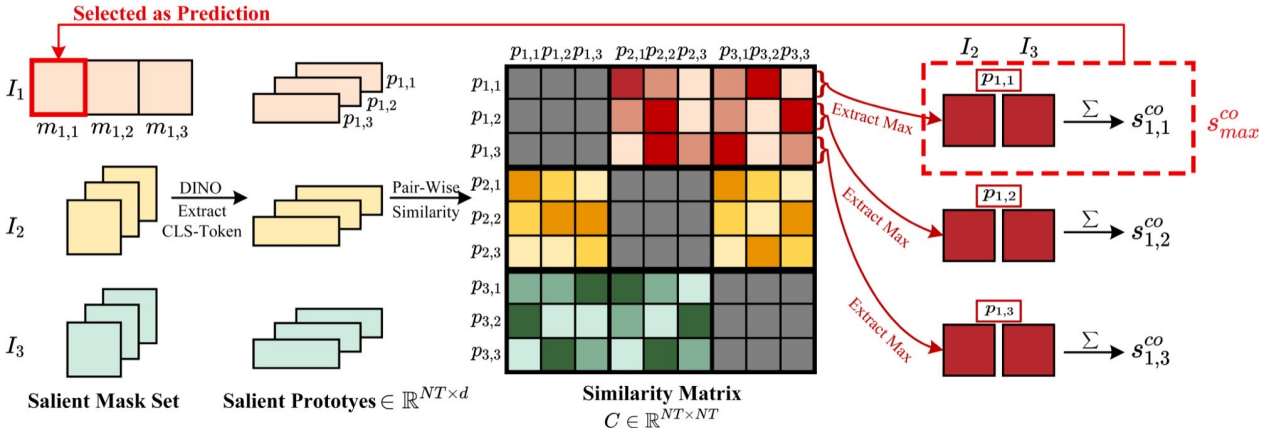

Figure 5. Illustration of Inter-image Prototype Selector (IPS) with an example of N=3 images and T=3 masks per image. A pairwise similarity matrix is constructed using mask prototypes, where different colors denote prototypes from different images. For each candidate (e.g., $p_{1,1}$ of image I_1), we select its maximum score (deep red cells) against the candidates from each of the other images (I_2 and I_3). These maximum scores are summed as the total co-saliency score s^{co}_{max}. The mask with the highest s^{co}_{max} is selected as the final prediction.

Next, we reshape the similarity matrix into $C \in \mathbb{R}^{NT\times N\times T}$. However, the similarity score within the same image can be ignored because it's not related to cross-image consistency. Thus, the size of the similarity matrix will become $C \in \mathbb{R}^{NT\times(N-1)\times T}$.

Then, we select the highest similarity score in each image except the target image to get the $N-1$ highest similarity scores for each prototype by:

$$C^{N-1_{max}} = \max_{i=\{1\cdots T\}} C[:,:,i], \tag{9}$$

where $C^{N-1_{max}} \in \mathbb{R}^{NT\times(N-1)}$. Afterwards, we derive the co-salient score $s^{co} \in \mathbb{R}^{NT}$ of each prototype by taking the sum of the $N-1$ highest similarity scores, which can be formulated as:

$$s^{co} = \sum_{n=1}^{N-1} C^{N-1_{max}}[:,n]. \tag{10}$$

Then, we reshape the co-salient score into $s^{co} \in \mathbb{R}^{N\times T}$, and choose the index of the prototype with the maximum co-salient score for each image:

$$s^{co}_{max} = \max_{t=\{1\cdots T\}} s^{co}[:,t], \tag{11}$$

$$index = ind(s^{co}_{max}), \tag{12}$$

where $ind(\cdot)$ means taking the index of the prototype with the maximum co-salient score.

Finally, the mask with the $index$ derived from Eq. 12 is selected as the final CoSOD prediction for each image. Through this progressive pipeline, our TF-SSD effectively transforms exhaustive mask proposals from SAM into precise co-salient masks across group images.

4. Experiments

4.1. Datasets and Evaluation Metrics

We conduct comprehensive experiments to verify the effectiveness on three widely-used benchmarks: CoCA [44], CoSal2015 [41], and CoSOD3k [8]. For evaluation, we employ several widely-used metrics: 1) F-measure ($F_\beta^{\max}$), which represents the harmonic mean of precision and recall values, calculated using a self-adaptive threshold. 2) S-measure (S_α), which is utilized to assess the spatial structural similarities of saliency maps. 3) Mean Absolute Error (MAE) that quantifies the average L1 distance between GT and predictions. 4) $E_\xi^{\max}$, a cognitive-based metric to capture both global statistics and local pixel-level similarity.

4.2. Implementation Details

Models and Environment. Our training-free framework is built upon two foundational models: SAM and DINO. Specifically, we utilize SAM [15] with a ViT-H backbone for mask generation and DINO [2, 25, 29] with a ViT-B/8 architecture for feature and attention map extraction, respectively. All experiments are conducted on a single NVIDIA 4090 GPU. For prototype extraction with DINO, the masked image regions are resized to 224x224 pixels.

Parameters. Our progressive pipeline involves several key hyperparameters that are discussed as follows:

- **Quality Mask Generator (QMG):** The initial area filtering threshold τ_{area} is set to 0.01. For overlap filtering, the threshold τ_{con} is set to 0.85. In the quality assessment stage, the ideal area range $[r_{min}, r_{max}]$ is set to [0.15, 0.7], with the parameters $\sigma = 0.7$ and $\gamma = 1.5$. The weights of balanced quality score are $\alpha = 0.7$ and $\beta = 0.3$. We select the top $T_r = 10$ masks for next stage.

Table 1. **Quantitative comparisons between our TF-SSD and other methods.** "↑" ("↓") means that the higher (lower) is better. 'Type' denotes the various supervision settings, where 'S' denotes the supervised setting, 'U' denotes the unsupervised setting, and 'TF' denotes the training-free setting. Best results among training-free (TF) methods are marked **bold**.

Method	Pub. & Year	Type	CoCA [38]				CoSal2015 [41]				CoSOD3k [8]			
			MAE ↓	$F_\beta^{\max}$ ↑	$E_\xi^{\max}$ ↑	S_α ↑	MAE ↓	$F_\beta^{\max}$ ↑	$E_\xi^{\max}$ ↑	S_α ↑	MAE ↓	$F_\beta^{\max}$ ↑	$E_\xi^{\max}$ ↑	S_α ↑
DCFM [40]	CVPR 2022	S	0.085	0.598	0.783	0.710	0.067	0.856	0.892	0.838	0.067	0.805	0.874	0.810
CoRP [48]	TPAMI 2023	S	0.103	0.597	0.769	0.715	0.055	0.882	0.912	0.867	0.060	0.827	0.890	0.838
GCoNet+ [45]	TPAMI 2023	S	0.081	0.637	0.814	0.738	0.056	0.891	0.924	0.881	0.062	0.834	0.901	0.843
CONDA [20]	ECCV 2024	S	0.089	0.685	0.839	0.763	0.045	0.908	0.944	0.900	0.056	0.853	0.911	0.862
VCP [31]	CVPR 2025	S	0.069	0.680	0.829	0.774	0.037	0.920	0.944	0.911	0.049	0.868	0.868	0.874
TokenCut [32]	CVPR 2022	U	0.167	0.467	0.704	0.627	0.139	0.805	0.857	0.793	0.151	0.720	0.811	0.744
DVFDVD [1]	ECCVW 2022	U	0.223	0.422	0.592	0.592	0.092	0.777	0.842	0.809	0.104	0.722	0.819	0.773
US-CoSOD [4]	WACV 2024	U	0.116	0.546	0.743	0.672	0.070	0.845	0.886	0.840	0.076	0.779	0.861	0.801
SCoSPARC [3]	ECCV 2024	U	0.092	0.614	0.782	0.711	0.062	0.869	0.905	0.851	0.064	0.827	0.889	0.823
ZS-CoSOD [34]	ICASSP 2024	TF	0.115	0.549	-	0.667	0.101	0.799	-	0.785	0.117	0.691	-	0.723
TF-SSD (Ours)	Submission	TF	**0.077**	**0.686**	**0.815**	**0.763**	**0.089**	**0.899**	**0.926**	**0.890**	**0.090**	**0.860**	**0.908**	**0.861**

Table 2. **Ablation study of the proposed components in TF-SSD on three benchmark datasets.** QMG-1, QMG-2, and QMG-3 denote the three stages of our QMG, respectively. The final row represents our full framework. Best results are marked **bold**.

ID	Component					CoCA [44]				CoSal2015 [41]				CoSOD3k [8]			
	QMG-1	QMG-2	QMG-3	ISF	IPS	MAE ↓	F_β^{max} ↑	E_ξ^{max} ↑	S_α ↑	MAE ↓	F_β^{max} ↑	E_ξ^{max} ↑	S_α ↑	MAE ↓	F_β^{max} ↑	E_ξ^{max} ↑	S_α ↑
1	✓				✓	0.171	0.447	0.662	0.578	0.133	0.680	0.779	0.704	0.139	0.610	0.752	0.667
2	✓	✓			✓	0.121	0.497	0.747	0.650	0.095	0.815	0.875	0.799	0.099	0.744	0.839	0.754
3	✓	✓	✓		✓	0.119	0.522	0.765	0.634	0.092	0.850	0.900	0.818	0.099	0.785	0.862	0.786
5	✓	✓	✓	✓	✓	**0.077**	**0.686**	**0.815**	**0.763**	**0.089**	**0.899**	**0.926**	**0.890**	**0.090**	**0.860**	**0.908**	**0.861**

- **Intra-image Saliency Filter (ISF):** Based on the saliency score computed from DINO's attention map, we select the top $T = 6$ masks as salient ones for each image.

More details are provided in the supplementary materials.

4.3. Comparisons with State-of-the-art Methods

We compare our TF-SSD with existing SOTA methods under different settings, including fully-supervised methods: DCFM [40], CoRP [48], GCoNet+ [45], CONDA [20], VCP [31], unsupervised methods: TokenCut [32], DVFDVD [1], US-CoSOD [4], SCoSPARC [3], and a training-free approach, ZS-CoSOD [34].

Quantitive comparison. Tab. 1 illustrates comparison results. It's observed that our TF-SSD outperforms all existing SOTA methods. Compared with the recent training-free method, ZS-CoSOD [34], our TF-SSD achieves gains of 3.8% for MAE, 13.7% for $F_\beta^{\max}$, and 9.6% for S_α on the CoCA benchmark. For other challenging real-world benchmarks, *i.e.*, CoSal2015 and CoSOD3k, our TF-SSD also gets promising performance. For example, TF-SSD achieves a gain of 1.2% for MAE, 10.0% for $F_\beta^{\max}$, and 10.5% for S_α on the CoSal2015 benchmark. In addition, our method achieves comparable performance to supervised learning methods and outperforms unsupervised learning methods. For instance, TF-SSD achieves a gain of 3.0% for $F_\beta^{\max}$ and 3.9% for S_α on the CoSal2015 benchmark.

Qualitative comparison. Fig. 6 shows the visual comparison between TF-SSD and previous SOTA methods. Groups "Accordion" and "Chopsticks" are from the CoCA dataset. "Axe" is from the CoSal2015 dataset and "Baby_bed" is from the CoSOD3k dataset. It's observed that TF-SSD segments co-salient masks that align with the ground truth. Moreover, in complex cases, TF-SSD also predicts accurate masks. For example, in the group of slender characteristics, *i.e.*, "Chopsticks", TF-SSD predicts masks with smooth boundaries, while previous methods, no matter whether training-based or training-free methods, fail to accurately segment the co-salient target. In the case of "Baby_bed", TF-SSD also predicts better results than other training-based methods *i.e.*, GCoNet+ [45] and VCP [31]. These results demonstrate the strong capability of our TF-SSD.

4.4. Ablation Study

Effect of proposed components. Tab. 2 lists comprehensive ablation studies of each component in our TF-SSD. "QMG-1" denotes the SAM-based initial filtering, "QMG-2" denotes the overlap filtering and "QMG-3" denotes the quality assessment in our QMG. We treat the combination of QMG-1 and IPS as our baseline; otherwise, it is impossible to derive the final co-salient predictions. It can be observed that, through the initial filtering, the performance is quite poor, indicating that numerous noisy masks are pre-

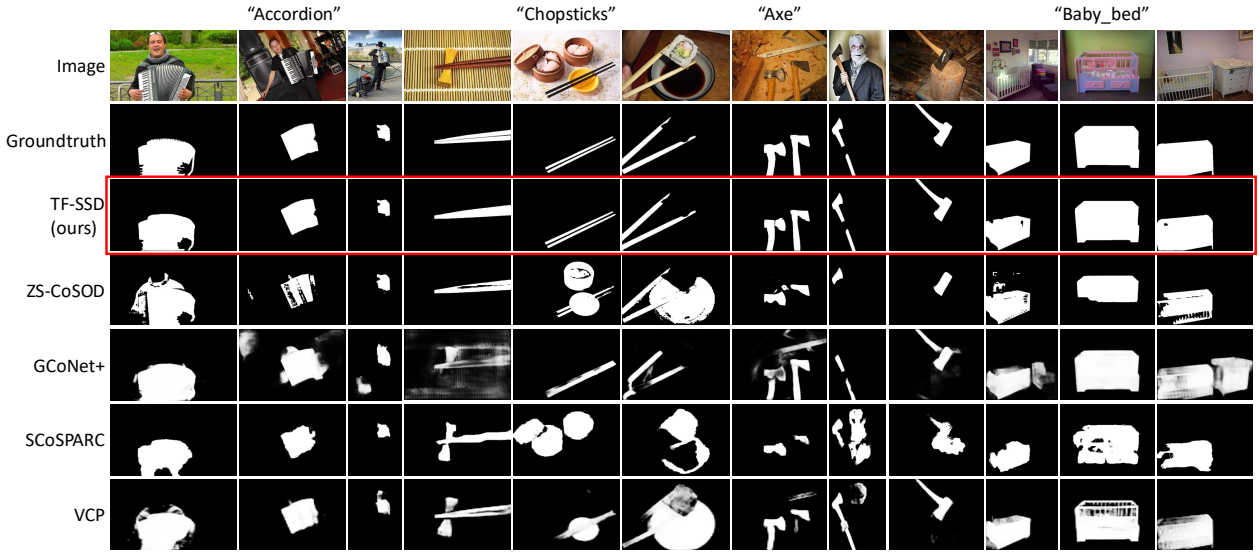

Figure 6. Qualitative comparison. We compare the result visualization between our method and previous SOTA methods. Among them, ZS-CoSOD [34] is the training-free method. GCoNet+ [45], VCP [31] and SCoSPARC [3] are training-based methods. It's observed that TF-SSD obtains precise co-salient masks compared to other SOTA methods, even in complicated cases (*e.g.*, "Chopsticks" and "Axe").

dicted by SAM. Then, with the help of QMG-2, the performance increases. After adding QMG-3, the first performance leap appears. It yields significant improvements across all evaluation metrics on all datasets. Finally, our ISF pushes the performance to SOTA, showing the importance of the saliency detection ability of DINO. For example, ISF brings a gain of 4.2% for MAE, 16.4% for $F_\beta^{\max}$, 5.0% for $E_\xi^{\max}$, and 12.9% for S_α on the CoCA dataset compared to row 3. Overall, they significantly contribute to our TF-SSD.

Table 3. **Ablation study of the $N-1$ similarity score selection (Eq. 9) in IPS.** We compare using the maximum similarity (*Max*) versus the average similarity (*Avg*) to compute the similarity score among cross-image prototypes.

Strategy	CoCA		CoSal2015		CoSOD3k	
	$F_\beta^{\max}\uparrow$	$E_\xi^{\max}\uparrow$	$F_\beta^{\max}\uparrow$	$E_\xi^{\max}\uparrow$	$F_\beta^{\max}\uparrow$	$E_\xi^{\max}\uparrow$
Avg	0.568	0.778	0.775	0.826	0.737	0.792
Max	**0.686**	**0.815**	**0.899**	**0.926**	**0.860**	**0.908**

Effect of selection strategy in IPS. Tab. 3 compares different selection strategies of the $N-1$ similarity score in Eq. 9. Our maximum similarity strategy (*Max*) is superior to averaging similarity (*Avg*), which yields a 12.4% gain in $F_\beta^{\max}$ on the CoSal2015 benchmark. This suggests that the maximum similarity exhibits strong semantic correlation across images with the same category.

Effect of threshold in ISF. Tab. 4 evaluates the number of setected salient masks in our ISF. It's observed that $T = 6$ provides the optimal trade-off between candidate recall and noise reduction. Moreover, if we narrow the number of selected masks, it exists over-filtering, while keeping too many masks introduces noise. It also suggests that it's worth exploring whether VFMs can provide better salient hints to extract more accurate semantic information for CoSOD.

Table 4. **Ablation study on the number of selected masks (T) in the ISF module**. Performance is evaluated on the CoCA dataset.

T	MAE $\downarrow$	$F_\beta^{\max}\uparrow$	$E_\xi^{\max}\uparrow$	$S_\alpha\uparrow$
10	0.078	0.616	0.786	0.718
8	0.078	0.645	0.789	0.726
7	0.077	0.666	0.809	0.744
6	**0.077**	**0.686**	**0.815**	**0.763**
5	0.077	0.667	0.804	0.748

5. Conclusion

In this paper, we introduce a novel method, TF-SSD, to address CoSOD in a training-free manner. First, it employs SAM to acquire a candidate mask pool and introduces a quality mask generator to filter out redundant masks. Then, an intra-image saliency filter is adopted to identify the salient objects within images. Moreover, TF-SSD proposes an inter-image prototype selector that models the co-saliency relations to select the most related masks as the final prediction for CoSOD. Extensive experiments demonstrate that our method achieves significant gains. TF-SSD presents a new paradigm that explores salient semantic understanding upon VFM results, and we envision it serving as a strong baseline to facilitate future research.

Acknowledgment

This work was supported by the National Natural Science Foundation of China (No. 62301451, 62301613, 62471405, 62331003), Basic Research Program of Jiangsu (BK20241814), Suzhou Basic Research Program (SYG202316), XJTLU REF-22-01-010 and XJTLU RDF-22-02-066.

References

[1] Shir Amir, Yossi Gandelsman, Shai Bagon, and Tali Dekel. Deep vit features as dense visual descriptors. *arXiv preprint arXiv:2112.05814*, 2021. 2, 3, 7

[2] Mathilde Caron, Hugo Touvron, Ishan Misra, Hervé Jégou, Julien Mairal, Piotr Bojanowski, and Armand Joulin. Emerging properties in self-supervised vision transformers. In *ICCV*, pages 9650–9660, 2021. 1, 2, 3, 6, 11

[3] Souradeep Chakraborty and Dimitris Samaras. Self-supervised co-salient object detection via feature correspondences at multiple scales. In *ECCV*, pages 231–250, 2024. 3, 7, 8

[4] Souradeep Chakraborty, Shujon Naha, Muhammet Bastan, Amit Kumar K. C., and Dimitris Samaras. Unsupervised and semi-supervised co-salient object detection via segmentation frequency statistics. In *WACV*, pages 332–342, 2024. 2, 3, 7

[5] Jia Deng, Wei Dong, Richard Socher, Li-Jia Li, Kai Li, and Li Fei-Fei. ImageNet: A large-scale hierarchical image database. In *CVPR*, pages 248–255, 2009. 3

[6] Zheng Ding, Jieke Wang, and Zhuowen Tu. Open-vocabulary panoptic segmentation with maskclip. *arXiv preprint arXiv:2208.08984*, 2022. 3

[7] Deng-Ping Fan, Zheng Lin, Ge-Peng Ji, Dingwen Zhang, Huazhu Fu, and Ming-Ming Cheng. Taking a deeper look at co-salient object detection. In *CVPR*, pages 2919–2929, 2020. 1, 11

[8] Deng-Ping Fan, Tengpeng Li, Zheng Lin, Ge-Peng Ji, Dingwen Zhang, Ming-Ming Cheng, Huazhu Fu, and Jianbing Shen. Re-thinking co-salient object detection. *IEEE T-PAMI*, 44(8):4339–4354, 2021. 6, 7

[9] Yanliang Ge, Qiao Zhang, Tian-Zhu Xiang, Cong Zhang, and Hongbo Bi. Tcnet: Co-salient object detection via parallel interaction of transformers and cnns. *IEEE T-CSVT*, 2022. 2

[10] Kaiming He, Xinlei Chen, Saining Xie, Yanghao Li, Piotr Dollár, and Ross Girshick. Masked autoencoders are scalable vision learners. In *CVPR*, 2022. 3

[11] Qibin Hou, Ming-Ming Cheng, Xiaowei Hu, Ali Borji, Zhuowen Tu, and Philip HS Torr. Deeply supervised salient object detection with short connections. In *CVPR*, pages 3203–3212, 2017. 2

[12] Kuang-Jui Hsu, Yen-Yu Lin, Yung-Yu Chuang, et al. Co-attention cnns for unsupervised object co-segmentation. In *IJCAI*, page 2, 2018. 2

[13] Shuo Jin, Meiqin Liu, Chao Yao, Chunyu Lin, and Yao Zhao. Kernel dimension matters: To activate available kernels for real-time video super-resolution. In *ACMMM*, pages 8617–8625, 2023. 3

[14] Shuo Jin, Siyue Yu, Bingfeng Zhang, Mingjie Sun, Yi Dong, and Jimin Xiao. Feature purification matters: Suppressing outlier propagation for training-free open-vocabulary semantic segmentation. In *ICCV*, pages 20291–20300, 2025. 3

[15] Alexander Kirillov, Eric Mintun, Nikhila Ravi, Hanzi Mao, Chloe Rolland, Laura Gustafson, Tete Xiao, Spencer Whitehead, Alexander C Berg, Wan-Yen Lo, et al. Segment anything. In *ICCV*, pages 4015–4026, 2023. 1, 3, 6, 11

[16] Hieu Le, Chen-Ping Yu, Gregory Zelinsky, and Dimitris Samaras. Co-localization with category-consistent features and geodesic distance propagation. In *ICCVW*, pages 1103–1112, 2017. 2

[17] Guanbin Li and Yizhou Yu. Deep contrast learning for salient object detection. In *CVPR*, pages 478–487, 2016. 2

[18] Junnan Li, Dongxu Li, Caiming Xiong, and Steven Hoi. Blip: Bootstrapping language-image pre-training for unified vision-language understanding and generation. In *ICML*, pages 12888–12900, 2022. 3

[19] Long Li, Junwei Han, Ni Zhang, Nian Liu, Salman Khan, Hisham Cholakkal, Rao Muhammad Anwer, and Fahad Shahbaz Khan. Discriminative co-saliency and background mining transformer for co-salient object detection. In *CVPR*, pages 7247–7256, 2023. 2

[20] Long Li, Nian Liu, Dingwen Zhang, Zhongyu Li, Salman Khan, Rao Anwer, Hisham Cholakkal, Junwei Han, and Fahad Shahbaz Khan. Conda: Condensed deep association learning for co-salient object detection. In *ECCV*, pages 287–303, 2024. 7

[21] Jiawei Liu, Jing Zhang, and Nick Barnes. Semi-supervised salient object detection with effective confidence estimation. *arXiv preprint arXiv:2112.14019*, 2021. 2

[22] Meiqin Liu, Shuo Jin, Chao Yao, Chunyu Lin, and Yao Zhao. Temporal consistency learning of inter-frames for video super-resolution. *IEEE T-CSVT*, 33(4):1507–1520, 2022. 3

[23] Yan Liu, Tengpeng Li, Yang Wu, Huihui Song, and Kaihua Zhang. Self-supervised image co-saliency detection. *Computers and Electrical Engineering*, 105:108533, 2023. 2

[24] Pedro O O Pinheiro, Amjad Almahairi, Ryan Benmalek, Florian Golemo, and Aaron C Courville. Unsupervised learning of dense visual representations. In *NeurIPS*, 2020. 3

[25] Maxime Oquab, Timothée Darcet, Théo Moutakanni, Huy Vo, Marc Szafraniec, Vasil Khalidov, Pierre Fernandez, Daniel Haziza, Francisco Massa, Alaaeldin El-Nouby, et al. Dinov2: Learning robust visual features without supervision. *arXiv preprint arXiv:2304.07193*, 2023. 1, 2, 3, 6, 11

[26] Alec Radford, Jong Wook Kim, Chris Hallacy, Aditya Ramesh, Gabriel Goh, Sandhini Agarwal, Girish Sastry, Amanda Askell, Pamela Mishkin, Jack Clark, et al. Learning transferable visual models from natural language supervision. In *ICML*, pages 8748–8763, 2021. 3

[27] Nikhila Ravi, Valentin Gabeur, Yuan-Ting Hu, Ronghang Hu, Chaitanya Ryali, Tengyu Ma, Haitham Khedr, Roman Rädle, Chloe Rolland, Laura Gustafson, et al. Sam 2: Segment anything in images and videos. *arXiv preprint arXiv:2408.00714*, 2024. 3

[28] Shuai Shao, Zeming Li, Tianyuan Zhang, Chao Peng, Gang Yu, Xiangyu Zhang, Jing Li, and Jian Sun. Objects365:

A large-scale, high-quality dataset for object detection. In *ICCV*, pages 8430–8439, 2019. 3

[29] Oriane Siméoni, Huy V Vo, Maximilian Seitzer, Federico Baldassarre, Maxime Oquab, Cijo Jose, Vasil Khalidov, Marc Szafraniec, Seungeun Yi, Michaël Ramamonjisoa, et al. Dinov3. *arXiv preprint arXiv:2508.10104*, 2025. 2, 3, 6

[30] Sagar Vaze, Kai Han, Andrea Vedaldi, and Andrew Zisserman. Generalized category discovery. In *CVPR*, pages 7492–7501, 2022. 2

[31] Jie Wang, Nana Yu, Zihao Zhang, and Yahong Han. Visual consensus prompting for co-salient object detection. In *CVPR*, pages 9591–9600, 2025. 3, 7, 8

[32] Yangtao Wang, Xi Shen, Yuan Yuan, Yuming Du, Maomao Li, Shell Xu Hu, James L Crowley, and Dominique Vaufreydaz. Tokencut: Segmenting objects in images and videos with self-supervised transformer and normalized cut. *IEEE T-PAMI*, 2023. 2, 3, 7

[33] Yang Wu, Huihui Song, Bo Liu, Kaihua Zhang, and Dong Liu. Co-salient object detection with uncertainty-aware group exchange-masking. In *CVPR*, pages 19639–19648, 2023. 2

[34] Haoke Xiao, Lv Tang, Bo Li, Zhiming Luo, and Shaozi Li. Zero-shot co-salient object detection framework. In *ICASSP*, pages 4010–4014, 2024. 1, 2, 3, 7, 8

[35] Peiran Xu and Yadong Mu. Co-salient object detection with semantic-level consensus extraction and dispersion. In *ACMM*, pages 2744–2755, 2023. 2

[36] Haochen Xue, Feilong Tang, Ming Hu, Yexin Liu, Qidong Huang, Yulong Li, Chengzhi Liu, Zhongxing Xu, Chong Zhang, Chun-Mei Feng, et al. Mmrc: A large-scale benchmark for understanding multimodal large language model in real-world conversation. *arXiv preprint arXiv:2502.11903*, 2025. 3

[37] Pengxiang Yan, Ziyi Wu, Mengmeng Liu, Kun Zeng, Liang Lin, and Guanbin Li. Unsupervised domain adaptive salient object detection through uncertainty-aware pseudo-label learning. In *AAAI*, pages 3000–3008, 2022. 2

[38] Jiahui Yu, Zirui Wang, Vijay Vasudevan, Legg Yeung, Mojtaba Seyedhosseini, and Yonghui Wu. Coca: Contrastive captioners are image-text foundation models. *arXiv preprint arXiv:2205.01917*, 2022. 7

[39] Jizhe Yu, Xiya Bu, Yu Liu, and Kaiping Xu. Pap-sam: Global-local prior adaptive perception sam for co-salient object detection. In *Proceedings of the 2025 International Conference on Multimedia Retrieval*, pages 1720–1729, 2025. 3

[40] Siyue Yu, Jimin Xiao, Bingfeng Zhang, and Eng Gee Lim. Democracy does matter: Comprehensive feature mining for co-salient object detection. In *CVPR*, pages 979–988, 2022. 7

[41] Dingwen Zhang, Junwei Han, Chao Li, and Jingdong Wang. Co-saliency detection via looking deep and wide. In *CVPR*, pages 2994–3002, 2015. 6, 7

[42] Kaihua Zhang, Yang Wu, Mingliang Dong, Bo Liu, Dong Liu, and Qingshan Liu. Deep object co-segmentation and co-saliency detection via high-order spatial-semantic network modulation. *IEEE T-MM*, 2022. 2

[43] Qijian Zhang, Runmin Cong, Junhui Hou, Chongyi Li, and Yao Zhao. Coadnet: Collaborative aggregation-and-distribution networks for co-salient object detection. *NeurIPS*, 33:6959–6970, 2020. 1

[44] Zhao Zhang, Wenda Jin, Jun Xu, and Ming-Ming Cheng. Gradient-induced co-saliency detection. In *ECCV*, pages 455–472, 2020. 2, 6, 7

[45] Peng Zheng, Huazhu Fu, Deng-Ping Fan, Qi Fan, Jie Qin, Yu-Wing Tai, Chi-Keung Tang, and Luc Van Gool. Gconet+: A stronger group collaborative co-salient object detector. *IEEE T-PAMI*, 45(9):10929–10946, 2023. 2, 3, 7, 8

[46] Peng Zheng, Jie Qin, Shuo Wang, Tian-Zhu Xiang, and Huan Xiong. Memory-aided contrastive consensus learning for co-salient object detection. In *AAAI*, pages 3687–3695, 2023. 2

[47] Jinghao Zhou, Chen Wei, Huiyu Wang, Wei Shen, Cihang Xie, Alan Yuille, and Tao Kong. ibot: Image bert pre-training with online tokenizer. *arXiv preprint arXiv:2111.07832*, 2021. 3

[48] Ziyue Zhu, Zhao Zhang, Zheng Lin, Xing Sun, and Ming-Ming Cheng. Co-salient object detection with co-representation purification. *IEEE T-PAMI*, 45(7):8193–8205, 2023. 2, 7

6. Supplementary Materials

This supplementary material provides additional details to complement our main paper. We elaborate on our implementation details in Sec. 7, present more quantitative and qualitative results in Sec. 8 and Sec. 9, and discuss the limitations of our method in Sec. 10.

7. Additional implementation details

To handle challenging cases, several mechanisms are necessary to ensure robustness in practice. Due to space limitations in the main paper, we describe these details below.

7.1. Fallback mechanism in ISF

Our Intra-image Saliency Filter (ISF) relies on DINO's attention maps to identify salient objects from SAM [15] proposals. However, in some challenging scenarios, QMG may fail to segment salient masks, where all masks yield low saliency scores $s_{n,t}^{sal}$. To ensure robustness, we employ a fallback mechanism that directly generates masks from attention maps to avoid these bad cases.

In particular, if the maximum saliency score $\max_t(s_{n,t}^{sal})$ is lower than a threshold τ_{fb}, the attention map $\mathcal{A}_n$ is binarized to obtain a mask $m_{n,t}^{fb}$ that captures the salient region, formulated as:

$$m_{n,t}^{fb}(x,y) = \begin{cases} 1 & \text{if } A_n(x,y) > \tau_{attn}, \\ 0 & \text{otherwise}, \end{cases} \tag{13}$$

where τ_{attn} is the binarization threshold for $\mathcal{A}_n$. This single fallback mask $m_{n,t}^{fb}$ will replace the low-quality masks. This operation ensures that each image retains at least one salient candidate mask for subsequent processing. In our implementation, we set $\tau_{fb} = 0.05$, and τ_{attn} is dynamically set to a threshold that retains the top 50% of the highest attention values for each map $\mathcal{A}_n$.

7.2. Merging of multiple co-salient objects in IPS

Our Inter-image Prototype Selector (IPS) is designed to identify the target co-salient object in each image. However, individual images may contain multiple instances of the co-salient object, and SAM often segments them separately. To obtain accurate results for CoSOD, we have to merge these separate masks into a single one.

To address such cases, we employ a dual-verification mechanism with two thresholds: a semantic similarity threshold τ_{sem} and a consistency difference threshold τ_{diff}. For each image I_n with a selected mask $\hat{m}_n$, we examine the remaining masks in $\mathcal{M}_n^{salient}$ to identify extra co-salient objects. A candidate mask m_j is considered an extra co-salient object if it satisfies the following two conditions:

1) **Semantic similarity:** The candidate mask is semantically similar to the primary mask, measured by pairwise similarity $\langle p_{\hat{m}_n}, p_j \rangle \geq \tau_{sem}$.

Table 5. Ablation study on different area ratio thresholds τ_{area} on the CoCA dataset.

τ_{area}	$F_\beta^{\max}$	Oracle $F_\beta^{\max}$
0.002	0.545	0.696
0.005	0.601	0.722
0.01	**0.686**	**0.768**
0.02	0.653	0.737

2) **Cross-image consistency:** The candidate mask exhibits comparable cross-image consistency, measured by $|S_j^{co} - S_{\hat{m}_n}^{co}| < \tau_{diff}$.

The first condition ensures semantic coherence within the image, while the second verifies that the candidate mask represents an object that appears consistently across the group. Verified masks are merged with the primary mask to form the final segmentation mask. In our implementation, τ_{sem} is dynamically set as the top 80% of intra-image pairwise similarities, and τ_{diff} is set to 0.1.

8. Additional quantitative results

8.1. Different SAM area ratios

The area ratio threshold τ_{area} is a critical parameter in our QMG that filters out excessively small masks (Eq. 2 in the main paper). To evaluate its impact on CoSOD performance, we conduct ablation experiments with four different threshold values: 0.002, 0.005, 0.01, and 0.02 on the CoCA [7] dataset. We employ two metrics: (1) **F-measure**: the final CoSOD performance obtained using the complete TF-SSD framework; (2) **Oracle F**: the upper bound performance computed using selected oracle masks from QMG.

As shown in Tab. 5, when the threshold is too low (0.005), excessive trivial masks are retained in the candidate set, introducing noise that degrades the subsequent ISF and IPS. Meanwhile, the Oracle F score reflects the quality of the candidate pool. When the threshold is too high (0.02), some valid co-salient objects are incorrectly filtered out, which limits both the quality of the candidate pool and the final performance. $\tau_{area} = 0.01$ strikes an optimal balance, which effectively removes trivial masks while preserving diverse co-salient object candidates.

8.2. Performance using other DINO backbones

Our main experiments use DINO ViT-B/8 [2] as the backbone for feature extraction in ISF. To provide a broader performance assessment, we compare it with two other notable backbones: (1) ViT-B/16 [2] from the same DINO framework with a larger patch size; (2) ViT-B/14 [25] from the more recent DINOv2 framework. We conduct experiments on the CoCA dataset, which highlights the trade-offs between different DINO versions.

As shown in Tab. 6, DINO ViT-B/8 significantly outperforms other configurations across all three metrics. A smaller patch size enables our model to capture finer spatial details, which is crucial for feature matching and prototype selection in our ISF and IPS. In contrast, although DINOv2 ViT-B/14 utilizes more advanced pretraining strategies, its larger patch size limits the perception of fine-grained information. This result demonstrates that a smaller patch size is more suitable for CoSOD that require precise localization and fine-grained feature alignment.

Table 6. Performance comparison of different DINO backbones on the CoCA dataset.

Backbone	$F_\beta^{\max}$	$E_\xi^{\max}$	S_α
DINO ViT-B/16	0.556	0.742	0.697
DINOv2 ViT-B/14	0.607	0.783	0.708
DINO ViT-B/8	**0.686**	**0.815**	**0.763**

8.3. Ablation on hyperparameter settings

We conduct additional ablation studies to evaluate the impact of hyperparameter settings.

Quality score weights. The balanced quality score $S_{n,t}^{ba}$ (Eq. 5 in the main paper) combines IoU prediction confidence and area preference through weights α and β, where $\alpha + \beta = 1$ to ensure normalized weighting between the two terms. Tab. 7 illustrates the performance with different weight settings on the CoCA dataset.

Table 7. Ablation on quality score weights on the CoCA dataset.

α	β	$F_\beta^{\max}$	$E_\xi^{\max}$	S_α
0.0	1.0	0.473	0.702	0.611
0.3	0.7	0.591	0.737	0.651
0.5	0.5	0.658	0.795	0.744
0.7	**0.3**	**0.686**	**0.815**	**0.763**
1.0	0.0	0.641	0.782	0.735

Ideal size range. The ideal size range $[r_{min}, r_{max}]$ (Eq. 4 in the main paper) defines the appropriate size for co-salient objects. Tab. 8 presents results for different range settings. The range $[0.15, 0.7]$ performs best, suggesting that co-salient objects typically occupy 15%-70% of the image area. More restrictive ranges (*e.g.* [0.2, 0.5]) limit the number of valid masks, while much wider ranges (*e.g.* [0.05, 0.85]) fail to effectively filter out background and large masks.

Overlap threshold. The overlap threshold τ_{con} controls how aggressively overlapping masks are filtered. As shown in Tab. 9, $\tau_{con} = 0.85$ achieves the optimal performance. Lower thresholds (*e.g.*, 0.5) retain too many redundant masks, while higher thresholds (*e.g.*, 0.95) will incorrectly remove valid masks that partially overlap with larger objects. They both lead to the reduced diversity of candidate masks for subsequent processing.

Table 8. Ablation on ideal size range on the CoCA dataset.

r_{min}	r_{max}	$F_\beta^{\max}$	$E_\xi^{\max}$	S_α
0.05	0.85	0.661	0.798	0.747
0.1	0.6	0.678	0.808	0.756
0.15	**0.7**	**0.686**	**0.815**	**0.763**
0.2	0.5	0.619	0.741	0.669

Table 9. Ablation on overlap threshold on the CoCA dataset.

τ_{con}	$F_\beta^{\max}$	$E_\xi^{\max}$	S_α
0.5	0.652	0.791	0.741
0.7	0.673	0.805	0.754
0.85	**0.686**	**0.815**	**0.763**
0.95	0.679	0.796	0.756

9. Additional qualitative results

In this section, we present visualizations of several key stages in our TF-SSD framework.

9.1. Visualization of SAM proposals

To demonstrate SAM's segmentation capability and the effectiveness of our QMG module, Fig. 7 visualizes the top-5 mask proposals ranked by our quality score $S_{n,t}^{ba}$ (Eq. 5 in the main paper). The masks with green borders represent our final predictions after the complete TF-SSD pipeline. It's observed that SAM can generate mask proposals that closely align with the GT, and our quality score $S_{n,t}^{ba}$ effectively ranks these masks at the top positions. It validates the effectiveness of SAM for mask generation and confirms that QMG can successfully identify promising candidate masks for subsequent processing.

9.2. Visualization of DINO attention maps

To illustrate the saliency-aware capability of DINO's attention mechanism, Fig. 8 visualizes the attention maps $\mathcal{A}_n$ of DINO's CLS-token. The attention maps can highlight the salient object regions that closely align with the GT masks. These observations validate the effectiveness of leveraging DINO attention maps to select salient mask proposals from the refined candidate set derived from our QMG.

10. Limitations

While our TF-SSD framework achieves strong performance on most CoSOD benchmarks, it still exhibits limitations in detecting small co-salient objects. As illustrated in Fig. 9, the "moon" category contains predominantly small objects

Figure 7. Visualization of SAM mask proposals for "Accordion" and "bicycle" image groups. For each group, we show the original images (row 1), ground truth(GT) masks (row 2), and the top-5 mask proposals ranked by quality score $S^{ba}_{n,t}$ (rows 3-7). Green borders indicate the final predictions selected by our TF-SSD pipeline.

that occupy a relatively small portion of the image. Due to SAM's initial area-based filtering mechanism in our QMG, masks with small area ratios ($r^{area}_{n,t} < \tau_{area}$) are typically denoted as trivial objects that are filtered out. In addition, small objects also tend to receive lower quality scores $S^{ba}_{n,t}$ from DINO's attention maps, which leads to wrong identification for co-salient objects.

Our future work concentrates on addressing these bad cases in challenging scenarios. We will explore incorporating semantic cues into an adaptive threshold that is modulated according to contexts of the image. We argue that it can identify the small salient objects from the trivial ones.

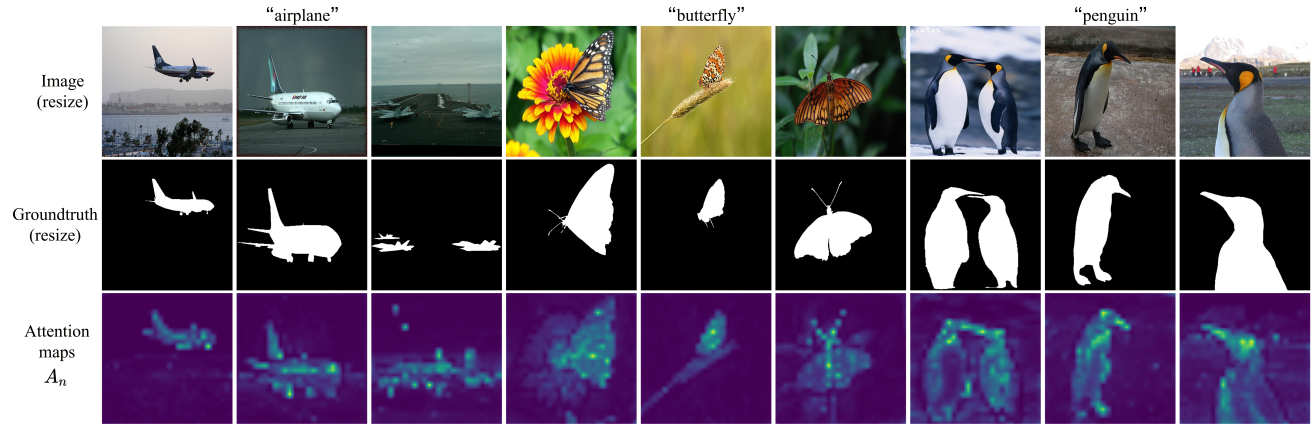

Figure 8. Visualization of DINO attention maps for three categories: ”airplane”, ”butterfly”, and ”penguin”. Row 1: Resized input images. Row 2: Resized GT masks. Row 3: DINO attention maps $\mathcal{A}_n$ that naturally highlight salient objects.

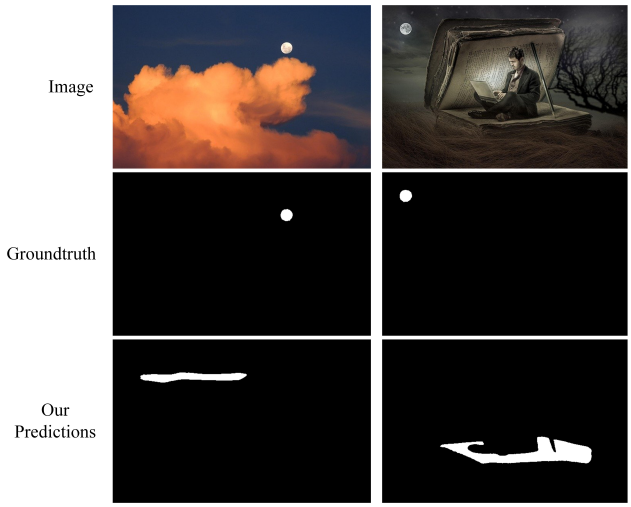

Figure 9. Limitation on small object detection. Visualizations of failed cases from the ”moon” category.